Flux flow in current driven mesoscopic superconductors: size effects

Pedro Nel Sánchez-Lotero
Programa de Pós-Graduaçao em Ciências de Materiais - CCEN, Universidade Federal de Pernambuco, Av. Jorn. Aníbal Fernandes s/n, 50740-560, Recife-PE, Brasil.

Daniel Domínguez
Centro Atómico Bariloche, 8400 San Carlos de Bariloche, Río Negro, Argentina.

J. Albino Aguiar
Departamento de Física, Universidade Federal de Pernambuco, Av. Jorn. Aníbal Fernandes s/n, 50740-560, Recife-PE, Brasil.

Flux-flow phenomena in a superconducting mesoscopic stripe submitted to an applied current and external magnetic field is studied. The time-dependent Ginzburg-Landau equations are solved numerically to obtain the electric and magnetic response of the system. It is shown that the I-V curves, for the wider strips, present an universal behaviour. The dependence of the flux-flow resistivity on the magnetic field and width allow us to propose a criterion characterizing, both, the macroscopic and mesoscopic regimes. The power spectrum of the average voltage permits identifying the effect of surface currents in vortices movement. Based on the maximum value of the power spectrum first harmonic we propose a geometric condition for matching between the sample dimensions and the vortex lattice parameter.

PACS numbers: VER: 74.78.Na, 74.40.+k, 74.20.De

I. INTRODUCTION

In a macroscopic superconductor the vortices arrange in a triangular lattice also called Abrikosov lattice[1]. In this lattice the most important interaction between vortices is due to the magnetic repulsion between them. However when the size of the superconductor decreases the interaction between the magnetic field of the vortices and the screening currents should be take in account. Additionally the usual boundary condition superconductor-vacuum allows the creation of the surface superconductivity with size of the coherence length. Boundary effects also modify the configuration of the vortex lattice. For example in small mesoscopic disks the circular geometry lead to the formation of concentric shells. When the radius of the disk is increased, more concentric shells appears but the inner shells starts to resemble an Abrikosov lattice[2]. This behaviour of vortex configurations was described theoretically using the molecular-dynamics simulations finding vortex configurations which are in agreement with those observed in the experiment[3]. This kind of analysis was performed in another superconducting symmetries. For example, theoretical and experimental results were obtained for square[4] and triangular[5] samples showing that the filling rules for vortices in these geometries, with increasing applied magnetic field, can be formulated in terms of formation of vortex shells. Even, in cases as large mesoscopic triangles[6] and thin disks with finite Λ[7] evidence of the influence of the symmetry in the vortex configuration is present. In existence of boundary defects, the competition between the confinement geometry and the geometric position of the defects leads to non-conventional vortex configurations which are distinct from the sample geometry[8]. For the case of a strip, the vortex lattice solutions also incorporate surface superconductivity. The vortex configuration is made of individual vortex rows parallel to the surfaces resembling an Abrikosov lattice when the width of the strip is increased[9]. In presence of an applied current the Lorentz force between the current and the magnetic flux of the lattice causes a continuous transverse movement of the vortices. For a mesoscopic strip with an applied current the vortices interact with the vortex lattice, the applied current and the screening currents. For a small applied current the vortices are pinned by the surface superconductivity but displaced from the center of the strip to one of the edges. Vortex flow starts at some finite current and the vortex structure is close to the triangular lattice. With increasing current, it transforms to a rowlike structure but keeping the triangular ordering. By further increasing the current, the number of vortex rows decreases and the number of vortices in the rows increases[10]. The moving vortices create an excess of quasiparticles behind themselves generating a wake of depleted order parameter. These vortices with a very anisotropic vortex core elongated in the direction of motion are called kinematic vortices. Each new vortice entering is attracted and interconnected to the previous one, creating the rowlike structure[11]. In a finite-length superconducting thin stripe with finite-size normal metal leads the moving vortex lattice becomes rearranged by the external current and fast and slow moving vortex channels are formed. Curved vortex channels are observed near normal contacts[12]. I-V measurements on wide thin Nb strips as a function of temperature and applied magnetic field show the intrinsic flux flow electronic instabilities of vortex motion[13] predicted by the Larkin-Ovchinnikov theory. For superconducting films

with a periodic array of antidots a transition from turbulent to laminarlike vortex flow has been found showing a negative differential resistivity in the current-voltage[14]. Kinematic vortices has been observed in superconducting samples with a periodic array of holes at high current densities by scanning Hall probe microscopy[15]. In superconducting films under an applied dc current it was analysed the influence of engineered pinning centers on the vortex velocity at which the flux-flow dissipation undergoes an abrupt transition from low to high resistance. For strongly disordered superconducting films, it was shown that, the mean critical vortex velocity for flux-flow instability has a nonmonotonic dependence on magnetic field and decreases as the pinning strength is increased[16]. Superconducting stripes with a periodic array of weakly-superconducting regions were studied finding different behaviour of vortices mobility in each region[17]. Opposite charged kinematic vortices have been predicted in mesoscopic superconducting loops[18] and submicron superconducting stripes in the presence of a longitudinal current[19]. These vortices can nucleate in the middle being expelled or enter on opposite sides and be annihilated in the middle of the stripe. Using the time-dependent Ginzburg-Landau in current-carrying superconductors magnetoresistance oscillations produced by the vortices movement have been predicted[20]. It was also studied the dynamics of flux-flow and phase slip states, and hot spot in a superconducting thin-film sample when abruptly a external current is switch on[21]. Finally the difference between the radiation produced by a single vortex or vortex bundle and a vortex lattice crossing a superconductor boundary were studied. For a moving vortex lattice coherent electromagnetic radiation should accompany the flux-flow state. The spectrum of the radiation has discrete character and extends up to the superconducting gap[22].

In this work we study the properties of flux-flow state in an infinite current-carrying superconducting strip for several strip widths. Both, the transition from microscopic to mesoscopic regime, in the presence of surface superconductivity, and the radiation spectrum as a function of the strip width are discussed.

II. MODEL

A. Time-dependent Ginzburg-Landau theory

As a model system, we use a bulk superconductor which is infinite in the z and x directions and is finite in the y direction (width=W). With this model we neglect the possibility of curved vortices in the z direction and, therefore, our problem becomes two dimensional. Our numerical simulations are carried out using the time-dependent Ginzburg-Landau (TDGL) equations. In the zero-electric potential gauge we have:[23]

$$\eta\frac{\partial}{\partial t}\Psi = (\vec{\nabla} - i\vec{A})^2\Psi + (1-|\Psi|^2)\Psi \qquad (1)$$

$$\frac{\partial}{\partial t}\vec{A} = \mathrm{Im}[\Psi^*(\nabla - i\vec{A})\Psi] - \kappa^2\vec{\nabla}\times\vec{\nabla}\times\vec{A}, \qquad (2)$$

where Ψ and $\vec{A}$ are the order parameter and vector potential respectively. Equations (1) and (2) are in their dimensionless form. Lengths have been scaled in units of the coherence length ξ, times in units of the Ginzburg-Landau relaxation time $t_0 = h/16k_B(Tc-T)\eta = \xi^2/\eta D$, magnetic field in units of the critical field H_{c2}, $\vec{A}$ in units of $H_{c2}\xi$, Ψ in units of $4k_BT_c\eta^{1/2}/\pi(1-T/T_c)^{1/2}$ and temperatures in units of the critical temperature T_c. D is the electron diffusion constant, k_B and h are the Boltzmann and Planck constants respectively. η is equal to the ratio of the characteristic time t_0 for the relaxation of $\vec{A}$ and the time t_{GL} for the relaxation of Ψ: $\eta = t_{GL}/t_0 = c^2/(4\pi\sigma_n\kappa^2 D)$, with $t_{GL} = \xi^2/D$, where σ_n is the quasiparticle conductivity. For superconductors with magnetic impurities $\eta = 12$, in our case we use $\eta = 5.79$[24]. The electric field is in units of $E_0 = \hbar/e^*\xi t_0$, voltages in units of $\hbar/e^*t_0$ and the current density per unit length in the z-direction J in units of $\hbar c^2/4\pi e^*\lambda^2\xi$ with λ the London penetration length. Periodic boundary conditions are applied in the x-direction: $\Psi(x) = \Psi(x+L)$ and $\vec{A}(x) = \vec{A}(x+L)$, where $L = 80\xi$ is the period. The usual superconductor-vacuum boundary conditions are applied in the y-direction

$$(\nabla_y - iA_y)\,|_{y=0,y=W} = 0 \qquad (3)$$

The transport current is introduced via the boundary condition for the vector potential in the y-direction, $\vec{\nabla}\times\vec{A}|_z(y=0, y=W) = H \pm H_{ind}$ where H is the applied magnetic field and $H_{ind} = 2\pi I/c$ is the magnetic field induced by the current per unit length in the z-direction, I. As the system voltage response is a time-dependent variable, we averaged it over a finite time interval which is taken to be larger than the period of the voltage variation. We solve the TDGL equations using a standard finite difference discretization scheme[23]. We consider a rectangular mesh consisting of $n_x \times n_y$ cells, with mesh spacings a_x and a_y. We use finite difference method based on gauge-invariant link variables[25]. This numerical method is defined by the finite unknowns of the method, Ψ, A_x, and A_y, plus the equations relating these unknowns. In what follows, we have solved the TDGL equations numerically for a type II superconductor with $\kappa = 2$. We used a spatial discretization of $\Delta x = \Delta y = 0.5\xi$ and, in order to make efficient calculations, we have chosen adequately the time step. We also include a thermal random force uncorrelated in space and time selected from a Gaussian distribution with a zero mean. Its standard deviation σ is given by

$$\sigma = \sqrt{\frac{2\pi}{\eta}E_r\Delta t(T/T_c)} \qquad (4)$$

where Δt is the time step and E_r is the ratio of the thermal energy to the free energy of a vortex ($E_r = 10^5$)[23].

III. RESULTS

For two different widths $W = 10\xi$ and $W = 66\xi$ and an applied magnetic field $H = 0.425H_{c2}$ we present the superconducting densities for some currents (Fig. 1 and Fig.2) and their current-voltage (J-E) characteristic, within the flux-flow regime. At $J = 0$, vortices arrange in structures that show the confinement effects of the small mesoscopic sample, In Fig. 1(a) there is a single vortex row for $W = 10\xi$, while in Fig. 2(a) for $W = 66\xi$, there is a nearly triangular structure in the center of the sample, with increasing defects when approaching the boundaries.

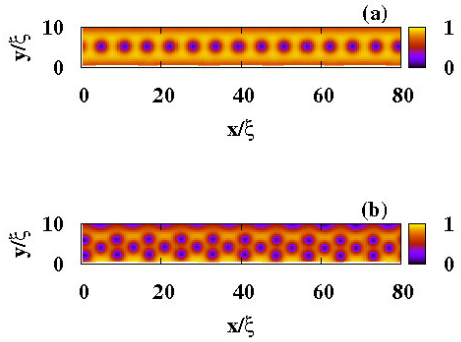

FIG. 1: Snapshots of the order parameter in the flux-flow regime for different values of the applied current, (a) $J = 0$, (b) $J > J_c$, and $W = 10\xi$ and $H = 0.425H_{c2}$.

Applying a current smaller than a critical current J_c, where J_c is the current for which the vortices start to move, it is induced the entrance of vortices into the sample, which rearrange in a new static structure with a higher vortex density. Above this critical current J_c, the vortex structure moves, and vortex motion helps to heal the lattice defects due to confinement in a finite sample. In Fig. 1(b) we can see three rows of vortices flowing in a $W = 10\xi$ sample at a current $J > J_c$. In Fig. 2(b) we see a nearly perfect triangular vortex lattice flowing in a larger sample with $W = 66\xi$. When increasing current, the effect of current-induced magnetic fields becomes increasingly important, inducing a gradient in vortex density, as it can be observed in Fig. 2(c). This density gradient introduces defects in the vortex lattice structure, which becomes important for increasing current. The magnitude of the current induced field is $B_{ind} \propto J$, being more important for large currents.

In Figs. 3(b) and 4(b) we can see that the field B increases with J in this regime. For a small sample ($W = 8\xi$) [Fig. 3(b)] jumps in B correspond to structural rearrangements after vortex entrance. On the other hand, large samples, [like $W = 51\xi$ in Fig. 4(b)] the field B, the magnetic induction, increases smoothly with current. Thus, the "ideal" flux flow regime of a triangular

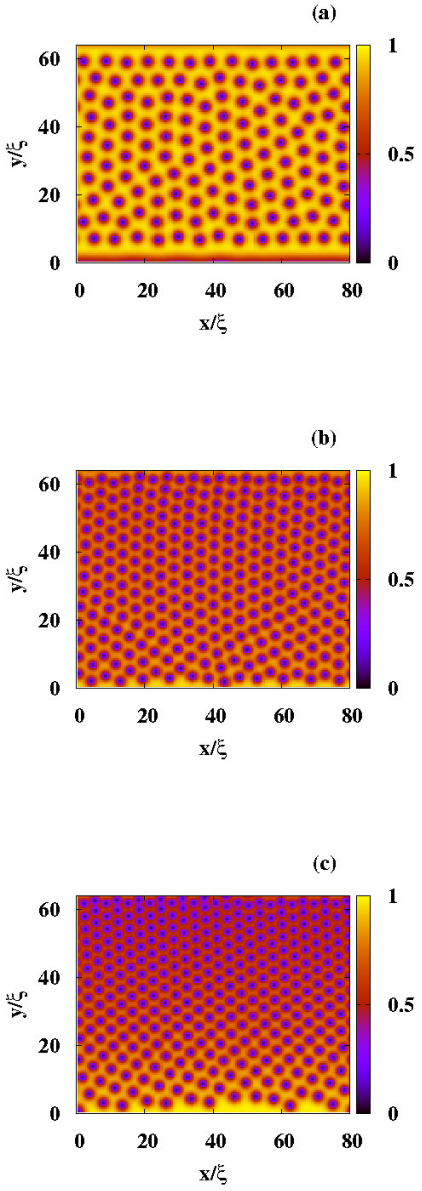

FIG. 2: Snapshots of the order parameter in the flux-flow regime for different values of the applied current within the flux-flow regime, for (a) $J = 0$, (b) $J = J_1 > J_c$, (c) $J = J_2$, with $J_1 > J_2$, and $W = 66\xi$ and $H = 0.425H_{c2}$.

lattice moving at constant speed can be found in a mesoscopic sample in a narrow region above the critical current J_c but below the current where the induced density gradient introduces important distortions in the lattice. In the case of Fig. 4, this corresponds to the range of currents where B is nearly constant with J and E is nearly linear with J. In the case of very small samples, like in Fig. 3, this flux flow regime is never achieved, since the effect of current induced fields is always relevant in this

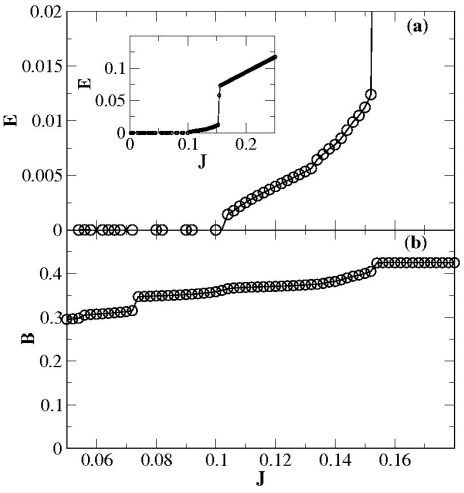

FIG. 3: (a) Longitudinal electric field as function of the current density with $H = 0.425H_{c2}$ and $W = 8\xi$. (b) Magnetic induction as function of the current density. Inset: Total E vs. J curve.

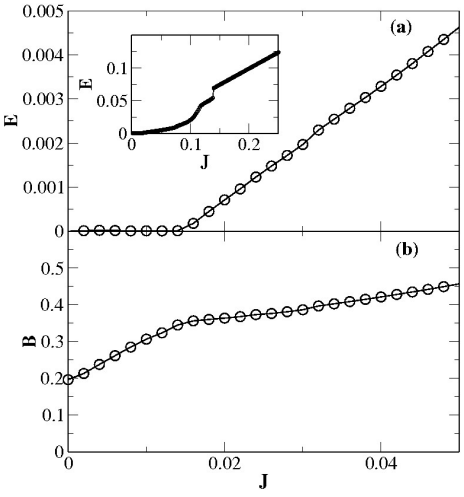

FIG. 4: (a) Longitudinal electric field as function of the current density with $H = 0.425H_{c2}$ and $W = 51\xi$. (b) Magnetic induction as function of the current density. Inset: Total E vs. J curve.

case.

A. I-V curves

J-E curves keeping fixed $H = 0.425H_{c2}$ and varying widths are shown in the Fig. 5. The critical current J_c is due to the nucleation of vortices at the edge of the sample when the edge magnetic field $H_{ind} = 2\pi I/c$ is of the order of the field H_p needed to overcome the surface barrier of the sample. Therefore, the critical current density depends on W as $J_c = I_c/W \propto H_p/W$. Then in Fig. 5 we

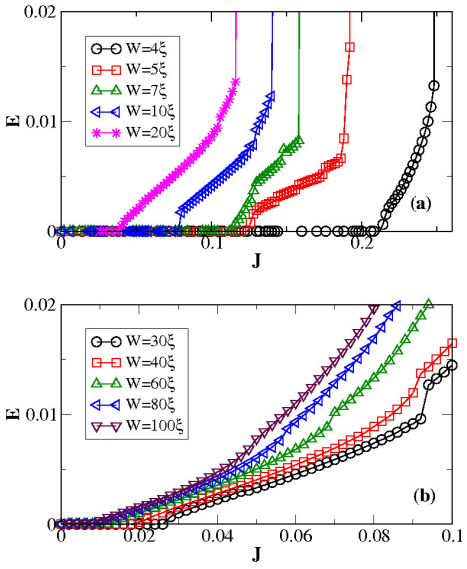

FIG. 5: J-E curve with $H = 0.425H_{c2}$. Upper panel for $W < 20\xi$ and lower one for $W > 20\xi$.

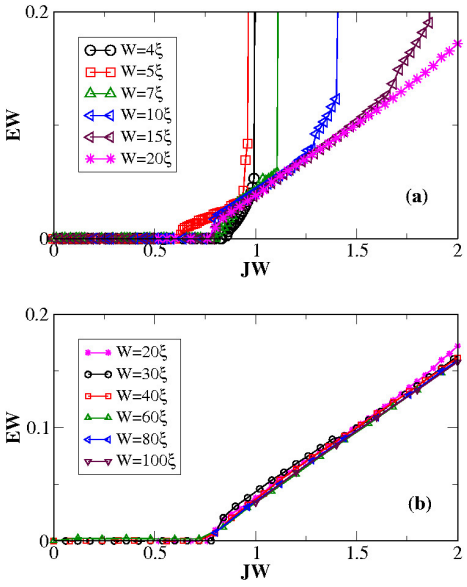

FIG. 6: $J.W$-$E.W$ curve with $H = 0.425H_{c2}$. Upper panel for $W < 20\xi$ and lower one for $W > 20\xi$.

see that the J-E curves move to the left when increasing W, since the critical current density decreases with W. Assuming that in the flux flow regime $E \approx \rho_{ff}(J - J_c)$, when plotting $E.W$ vs. $J.W$ one should get a single linear curve for the different widths W. We see in Fig. 6(b) that this linear scaling of the J-E curves is indeed obtained for $W > 20\xi$. On the other hand, as shown in Fig. 6(a), it is not possible to collapse the J-E curves for smaller sizes. In Fig. 7(a) we present the behaviour of the product $J_c.W \propto Hp$, as a function of the stripe

width W for several values of the applied field. It can be seen that for a fixed field and for large W ($W > 20\xi$), H_p is independent of width. On the other hand, for fixed W, H_p decreases with increasing magnetic field. We also obtained also the values for a critical current density, J_d, where the superconductivity disappears. As shown in Fig 7(b), for fixed magnetic field, J_d converges with increasing W, and also decreases for increasing magnetic field, for fixed width. It is necessary recall that our model is valid only for small values of the current although our results for J_d are consistent with the expected ones.

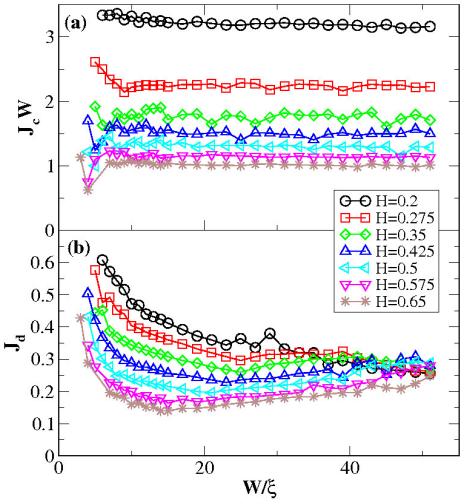

FIG. 7: Critical currents for different values of W. (a) Critical current density J_c for onset of voltage. (b) Current density for onset of normal state J_d.

B. Flux-flow regime

The relation between $\vec{E}$, the electric field, and the applied density current, $\vec{J}$ defines the flux-flow resistivity $\rho_{ff} = E/J = B\Phi_0/(\mu c^2)$, where Φ_0 is the quantum of magnetic flux and μ is the viscous coefficient. We calculated dE/dJ for different widths and fixed magnetic field. This ratio correspond to the slopes of the curves J-E in the flux flow regime [Fig. 8(a)]. dE/dJ curves present several plateau associated to different vortex configurations. The first plateau corresponds to the flux-flow regime. For smaller widths, in the flux-flow regime, we observe oscillations in dE/dJ, while for larger width dE/dJ becomes constant. By normalizing dE/dJ by B_{av}, the averaged magnetic induction, one see that all curves with for $W \geq 20\xi$ collapse, [Fig. 8(b)], as is expected for a macroscopic behaviour of the system[26].

C. Power spectrum and washboard frequency

As the number of vortices fluctuates due to incoming and outgoing of the vortices, thus the average voltage

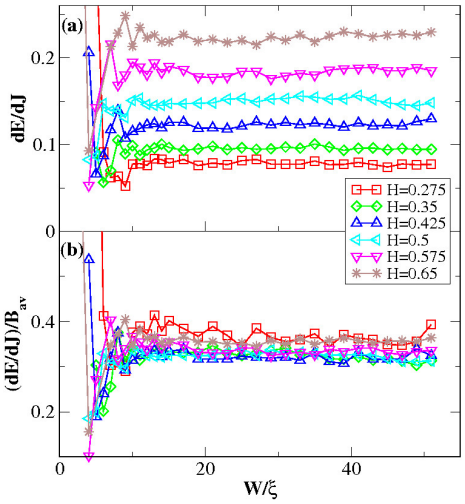

FIG. 8: Flux flow slopes vs. W. (a) dE/dJ vs. W for different H. (b) Flux flow slope normalized by B_{av} vs. W.

also shows fluctuations. In this way, the average voltage, in the direction of the applied current, depends on the vorticity of the system and its profile has a sequence of periodic pulses. These voltage pulses are related to the vortex motion. It is observed that a voltage pulse with a sharp peak is generated when a vortex appears or disappears at the boundaries[27]. Numerical simulations with similar results were reported previously describing these phenomena as caused by the intense surface current which gives rise to the effective strong force on vortices near the boundaries[29]. As the vortex motion and the electric field in the cores can be related to a time varying current which is associated to a potential difference through the a.c. Josephson effect in superconducting weak links[28], we obtained profiles of the average voltage as function of time for several widths for fixed applied magnetic and electric fields $H = 0.425H_{c2}$ and $E_x = 0.00548E_0$. For these profiles we calculated the power spectrum ($W = 18\xi$ and $W = 66\xi$, Fig. 9(a) and Fig. 9(b) respectively) obtaining an harmonic component group with periodicity in the frequency for the wider stripe, whereas for the smaller one only the first and second harmonic can be distinguished.

In Fig. 10(a) we see that for $W > 50\xi$ the first harmonic frequency ω_0 obtained from the power spectrum of $E(t)$, not presented, is independent of W. This shows that for large samples it corresponds to a washboard frequency. The washboard frequency for a perfect lattice moving at constant speed v is given by $\omega_0 = 2\pi v/a$, where a is the lattice constant and the speed v is given by $v = E/B$, an therefore ω_0 is size independent. On the other hand, the size dependence of ω_0 observed in Fig. 10(a) for small W is due to the fact that the time dependence of $E(t)$ is more affected by the entry and exit of vortices at the sample edges. In Fig. 10(b) it is shown the profile of the power spectrum value at washboard

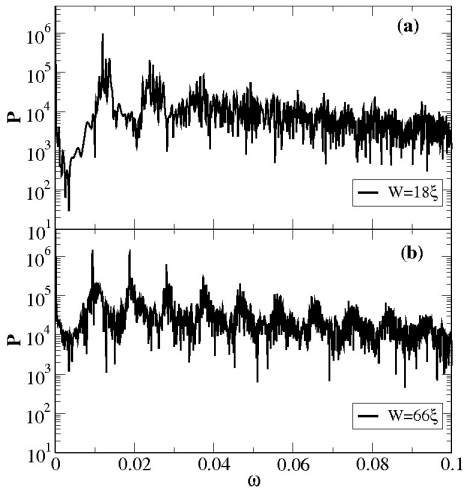

FIG. 9: Power spectra, for $H = 0.425H_{c2}$ within the flux-flow regime, fixed $E = 0.00548E_0$. (a) $W = 18\xi$. (b) $W = 66\xi$.

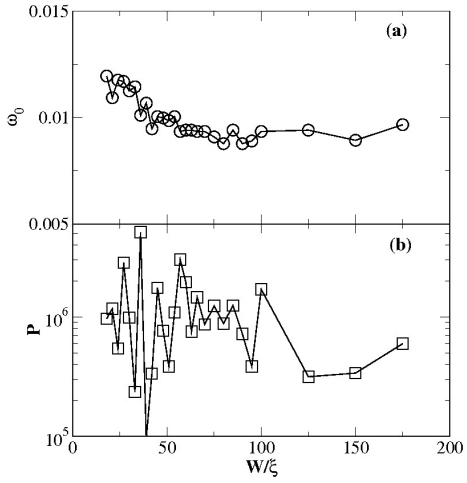

FIG. 10: Width dependence of the (a) washboard frequency ω_0 and (b) power at washboard frequency $P = P(\omega_0)$, at fixed E and H, for $H = 0.425H_{c2}$ and $E = 0.00548E_0$, within the flux-flow regime.

frequency. Again we observe two different behaviours depending of width. For small systems there are fluctuations in the value of the power spectrum maximum, while this feature is not observed for the wider samples. We assume that this behaviour is produced by a geometrical pinning which comes from the match between the width of the system and the lattice constant of the vortex lattice.

IV. SUMMARY AND CONCLUSIONS

In the framework of the time-dependent Ginzburg-Landau equations, we studied the flux-flow phenomena in a superconducting mesoscopic stripe submitted to an applied current and external magnetic field, for several stripe width W. We showed that above a critical current J_c the vortices move resembling a nearly perfect Abrikosov moving lattice. The flux-flow regime occurs in a narrow region between J_c and a current where an important distortion of the vortex structure is introduced. In this flux-flow regime, for sizes $W > 20\xi$ a linear scaling is obtained when plotting $E.W$ vs. $J.W$ whereas for smaller sizes this behaviour is not observed. Similar results are obtained when the flux-flow resistivity ρ_{ff} vs. W is plotted for several applied magnetic fields. From these results, we obtained a critical width that separate, both, the macroscopic and mesoscopic regimes. We also obtained, in the flux-flow regime, profiles of the average voltage vs. time for several widths and calculated their power spectrum. We found that for large W, the first harmonic frequency ω_0 obtained is independent of W. For small W the power spectrum is affected by the entry and exit of vortices at the sample edges. Based in the fluctuations of the first harmonic maximum we propose a geometric condition for matching between the sample dimensions and the vortex lattice parameter.

Acknowledgments

We thank M. V. Milošević for useful discussions and suggestions. This work was partially supported by the Brazilian agencies CAPES, CNPq, FACEPE (APQ C 0589/1.05-08): and Argentine ANPCyT (PICT2011-1537), CNEA and CONICET (PIP11220090100051).

[1] A. A. Abrikosov, Sov. Phys. JETP **32**, 1147 (1957).
[2] I. V. Grigorieva, W. Escoffier, J. Richardson, L. Y. Vinnikov, S. Dubonos, and V. Oboznov, Phys. Rev. Lett. **96**, 077005 (2006).
[3] V. R. Misko, B. Xu, and F. M. Peeters, Phys. Rev. B **76**, 024516 (2007).
[4] H. J. Zhao, V. R. Misko, F. M. Peeters, V. Oboznov, S. V. Dubonos, and I. V. Grigorieva, Phys. Rev. B **78**, 104517 (2008).
[5] H. J. Zhao, V. R. Misko, F. M. Peeters, S. Dubonos, V. Oboznov, and I. V. Grigorieva, EPL **83**, 17008 (2008); L. R. E. Cabral and J. Albino Aguiar, Phys. Rev. B **80**, 214533 (2009)
[6] L. R. E. Cabral and J. Albino Aguiar, Physica C **468**, 722 (2008).
[7] L. R. E. Cabral and J. Albino Aguiar, Physica C **460-462**, 1295 (2007).
[8] J. Barba-Ortega, E. Sardella, J. Albino Aguiar, and F. M. Peeters, Physica C **487**, 47 (2013).
[9] J. J. Palacios, Phys. Rev. B **57**, 10873 (1998); C. C. de

Souza Silva, L. R. E. Cabral and J. Albino Aguiar, Physica C **404**, 11 (2004)
[10] D. Y. Vodolazov and F. M. Peeters, Phys. Rev. B **76**, 014521 (2007).
[11] A. I. Larkin and Yu. N. Ovchinnikov, Sov. Phys. JETP **41**, 960 (1976).
[12] G. R. Berdiyorov, A. K. Elmurodov, F. M. Peeters, and D. Y. Vodolazov, Phys. Rev. B **79**, 174506 (2009).
[13] G. Grimaldi, A. Leo, C. Cirillo, C. Attanasio, A. Nigro, and S Pace, J. Phys.: Condens. Matter **21**, 254207 (2009).
[14] J. Gutiérrez, A. V. Silhanek, J. Van de Vondel, W. Gillijns, and V. V. Moshchalkov, Phys. Rev. B **80**, 140514(R) (2009).
[15] A. V. Silhanek, M. V. Milošević, R. B. G. Kramer, G. R. Berdiyorov, J. Van de Vondel, R. F. Luccas, T. Puig, F. M. Peeters, and V. V. Moshchalkov, Phys. Rev. Lett. **104**, 017001 (2010).
[16] A. V. Silhanek, A. Leo, G. Grimaldi, G. R. Berdiyorov, M. V. Milošević, A. Nigro, S. Pace, N. Verellen, W. Gillijns, V. Metlushko, B. Ilić, Xiaobin Zhu, and V. V. Moshchalkov, New Journal of Physics **14**, 053006 (2012).
[17] G. R. Berdiyorov, A. R. de C. Romaguera, M. V. Milošević, M. M. Doria, L. Covaci, and F. M. Peeters, Eur. Phys. J. B **85**, 130 (2012).
[18] G. R. Berdiyorov, M. V. Milošević, and F. M. Peeters, Physica C **470**, 946 (2010).
[19] G. R. Berdiyorov, M. V. Milošević, and F. M. Peeters, Phys. Rev. B **79**, 184506 (2009).
[20] G. R. Berdiyorov, X. H. Chao, F. M. Peeters, H. B. Wang, V. V. Moshchalkov, and B. Y. Zhu, Phys. Rev. B **86**, 224504 (2012).
[21] G. Berdiyorov, K. Harrabi, F. Oktasendra, K. Gasmi, A. I. Mansour, J. P. Maneval, and F. M. Peeters, Phys. Rev. B **90**, 054506 (2014).
[22] L. N. Bulaevskii and E. M. Chudnovsky, Phys. Rev. Lett. **97**, 197002 (2006).
[23] R. Kato, Y. Enomoto, and S. Maekawa, Phys. Rev. B **44**, 6916 (1991).
[24] L. Kramer and R. J. Watts-Tobin, Phys. Rev. Lett. **40**, 1041 (1978).
[25] G. Buscaglia, C. Bolech, and A. López, Connectivity and superconductivity, Lect. Notes Phys. **62**, 200 (2000).
[26] P. Sánchez-Lotero, J. Albino Aguiar, and D. Domínguez, Physica C. **503**, 120 (2014).
[27] D. J. van Ooijen and G. J. van Gurp, Phys. Lett. **17**, 230 (1965); B. Plaçais, P. Mathieu, and Y. Simon, Phys. Rev. Lett. **70**, 1521 (1993).
[28] B. B. Scwartz, Phys. Lett. **20**, 350 (1966).
[29] M. Machida and H. Kaburaki, Phys. Rev. Lett. **71**, 3206 (1993).